Research in Astronomy and Astrophysics, 22:085003 (15pp), 2022 August https://doi.org/10.1088/1674-4527/ac71a4

Candidate Eclipsing Binary Systems with a δ Scuti Star in Northern TESS Field

F. Kahraman Aliçavuş[1,2], D. Gümüş[3], Ö. Kırmızıtaş[4], Ö. Ekinci[5], S. Çavuş[4], Y. T. Kaya[6], and F. Aliçavuş[1,2]
[1] Çanakkale Onsekiz Mart University, Faculty of Sciences and Arts, Physics Department, 17100, Çanakkale, Turkey; filizkahraman01@gmail.com
[2] Çanakkale Onsekiz Mart University, Astrophysics Research Center and Ulupnar Observatory, TR-17100, Çanakkale, Turkey
[3] Istanbul University, Institute of Graduate Studies in Science, Programme of Astronomy and Space Sciences, 34116, Beyazıt, Istanbul, Turkey
[4] Çanakkale Onsekiz Mart University, School of Graduate Studies, Department of Physics, TR-17100, Çanakkale, Turkey
[5] Çanakkale Onsekiz Mart University, School of Graduate Studies, Department of Space Sciences and Technologies, TR-17100, Çanakkale, Turkey
[6] Çanakkale Onsekiz Mart University, Faculty of Engineering Computer Engineering, TR-17100, Çanakkale, Turkey
Received 2022 March 24; revised 2022 April 28; accepted 2022 May 10; published 2022 July 11

Abstract

The existence of pulsating stars in eclipsing binaries has been known for decades. These types of objects are extremely valuable systems for astronomical studies as they exhibit both eclipse and pulsation variations. The eclipsing binaries are the only way to directly measure the mass and radius of stars with a good accuracy ($\leqslant$1%), while the pulsations are a unique way to probe the stellar interior via oscillation frequencies. There are different types of pulsating stars existing in eclipsing binaries. One of them is the δ Scuti variables. Currently, the known number of δ Scuti stars in eclipsing binaries is around 90 according to the latest catalog of these variables. An increasing number of these kinds of variables is important to understand the stellar structure, evolution and the effect of binarity on the pulsations. Therefore, in this study, we focus on discovering new eclipsing binaries with δ Scuti component(s). We searched within the northern Transiting Exoplanet Survey Satellite (TESS) field with a visual inspection by following some criteria such as light curve shape, the existence of pulsation like variations in the out-of-eclipse light curve and the $T_{\rm eff}$ values of the targets. As a result of these criteria, we discovered some targets. The orbital variations were first removed from the TESS light curves and frequency analysis was performed on the residuals. The luminosity, and absolute and bolometric magnitudes of the targets were calculated as well. To find how much of these parameters represent the primary (more luminous) binary component, we also computed the flux density ratio of the systems by utilizing the area of the eclipses. In addition, the positions of the systems in the H-R diagram were examined considering the flux density ratios. As a consequence of the investigation, we defined 38 candidate δ Scuti stars and also one Maia variable in eclipsing binary systems.

Key words: (stars:) binaries: eclipsing – stars: variables: delta Scuti – techniques: photometric

Online material: machine-readable table

1. Introduction

Space telescopes have created a revolution in astronomical studies. The primary mission of some of these telescopes is mainly to discover new exoplanets, however, in addition to their success in finding new exoplanets, they have provided a huge amount of photometric data on stellar systems. Especially, the Kepler space telescope (Borucki et al. 2010) and the Transiting Exoplanet Survey Satellite (TESS, Ricker et al. 2014) have has a big impact on this. TESS has already finished its two-year primary mission and is currently continuing its extended mission by observing almost the entire sky. The high-quality photometric data of these space telescopes allow us to deeply investigate some phenomena in stellar systems and understand their structures.

To comprehend the evolution and structure of stars, the eclipsing binaries and pulsating stars are substantial systems. Eclipsing binaries are the only way to precisely determine the mass (M) and radius (R) parameters of the binary components with the help of modeling the photometric light curves and radial velocity measurements. The accuracy of the measured M and R values can be lower than 1% (Southworth 2013; Lacy et al. 2015). On the other hand, pulsating stars are unique systems that allow us to probe the stellar interior via oscillation frequencies (Aerts et al. 2010). Thanks to the analysis of high-quality space-based photometric data of pulsating stars, we had information on some important phenomena such as internal rotation, core overshooting and angular momentum (e.g., Saio et al. 2015; Lovekin & Guzik 2017). Therefore, the eclipsing binaries with a pulsating component(s) are crucial systems for deeply exploring stellar evolution and structure.

The presence of pulsating stars in eclipsing binaries has been known for decades (Tempesti 1971). There are different types of oscillating variables present in eclipsing binaries, for instance β Cephei, δ Scuti and γ Doradus stars (Lampens 2021; Southworth 2021). Currently, the known number of δ Scuti stars in eclipsing binaries (DSEBs) is higher than the other type of pulsating variables because of their relatively shorter pulsation periods (Kahraman Aliçavuş et al. 2017; Liakos & Niarchos 2017; Lampens 2021). The δ Scuti stars are early A- to F-type variables and their luminosity class changes from dwarf to giant (Aerts et al. 2010). These variables have their instability strip where theoretically δ Scuti-type variations are expected (Dupret et al. 2005). The δ Scuti stars generally exhibit pressure mode oscillation with an oscillation period range of 18 minutes to 8 hr (Aerts et al. 2010). According to the recent catalog of DSEBs, there are around 90 DSEBs (Kahraman Aliçavuş et al. 2017). Additionally, there are also δ Scuti stars present in other types of binary systems (Liakos & Niarchos 2017).

The effect of binarity on pulsations has been shown in some studies (Mkrtichian et al. 2004; Soydugan et al. 2006; Kahraman Aliçavuş et al. 2017; Handler et al. 2020). Because of the gravitational effects of the components on each other, it was expected that the pulsations in oscillating components differ from single pulsating stars. The effect of binarity on the pulsating δ Scuti components was shown by a relationship between the pulsation and orbital period (Soydugan et al. 2006). It was ascertained that the pulsation period ($P_{\rm puls}$) decreases when the orbital period ($P_{\rm orb}$) declines. The smaller $P_{\rm orb}$ means that the binary components are closer to each other, so the semimajor axis (a) is shorter. According to the law of gravity, applied gravitational force on the pulsating components is increased by the declined $P_{\rm orb}$. A comparison of the properties of single and eclipsing binary member δ Scuti stars was given by Kahraman Aliçavuş et al. (2017). They showed that $P_{\rm puls}$ and pulsation amplitude ($A_{\rm puls}$) of single classical δ Scuti stars are longer and higher, respectively, compared to eclipsing binary member δ Scuti variables. In this study, it is also presented that single δ Scuti stars have a higher rotation velocity ($v \sin i$) on average compared to DSEBs. These are the results of the effects of gravitational forces between the binary components. In the same study, some other relationships were examined between the pulsation properties ($P_{\rm puls}$, $A_{\rm puls}$) and other stellar parameters such as M, R, effective temperature ($T_{\rm eff}$) and surface gravity ($\log g$).

In a recent study, with the help of TESS data, Handler et al. (2020) for the first time showed that in a close binary system the pulsation axis of the oscillating component can be aligned by tidal forces. There are now a few samples of this kind of object including an eclipsing binary system and they are called "tidally tilted pulsators" (Fuller et al. 2020; Handler et al. 2020; Kurtz et al. 2020). The high-quality TESS data allowed us to find such variables which have been searched for years and have provided a good opportunity to deeply probe DSEBs. Comprehensive research on DSEBs is quite important for comprehending stellar structure, evolution and testing evolutionary models. For this reason, an increased number of such systems will offer us opportunities for understanding stellar objects. Hence, in this study, we focus on DSEBs.

In this study, we present our TESS northern field research for discovering new δ Scuti stars in eclipsing binaries. The paper is organized as follows. In Section 2, information about the observational data and target selection is introduced. In Section 3, the frequency analysis of the selected targets is given. In Section 4, calculations of some physical parameters and the position of the systems are presented. In Sections 5 and 6, discussion and conclusions are provided, respectively.

2. Observational Data and Target Selection

To discover new DSEBs, we searched for the northern TESS field. TESS was launched in April 2018 and its main goal is to detect exoplanets. TESS has four identical CCD cameras that each have a $24° \times 24°$ field of view (FOV) (Ricker et al. 2014). TESS monitors the sky with a wide red-bandpass filter by dividing it into sectors. Each sector has around 27 days of photometric observations. In the first two years of the mission, TESS observed many targets with 2 minute short cadence (SC) and 30 minute long cadence (LC) and now in its extended mission, LC was reduced to 10 minutes. According to the position of the target in the sky, some objects were observed by TESS in more than one sector while some have only one sector of data. The TESS data are public in the Barbara A. Mikulski Archive for Space Telescopes (MAST)[7] where the data are present in two kinds of fluxes; the simple aperture photometry (SAP) and the pre-search data conditioning SAP (PDCSAP) flux.

In the current study, to find new eclipsing binaries with a δ Scuti component, we performed a visual inspection of all TESS sectors in the northern hemisphere. Basically, in the first step, we searched for eclipsing binary like variations in the TESS data. In the next step, the out-of-eclipse variations of the determined eclipsing binaries were examined and the systems that exhibit both eclipsing binary variations and oscillation like changes in the out-of-eclipse light curves were chosen as targets. In the final step, the atmospheric parameters ($T_{\rm eff}$, $\log g$) of the targets were checked. As δ Scuti components are searched for, we regard targets as having $T_{\rm eff}$ and $\log g$ parameters in the range given for δ Scuti stars. According to the study of Rodríguez & Breger (2001), typical $T_{\rm eff}$ and $\log g$ ranges for δ Scuti stars are 6300–8500 K and 3.2–4.3, respectively. Therefore, for the final list, the targets having $T_{\rm eff}$ and $\log g$ in the given ranges within errors were chosen. The atmospheric parameters of the targets were taken from the TESS input catalog (TIC, Stassun et al. 2019). The final list of the targets is written in Table 1. There is one target (TIC 13037534) which has $T_{\rm eff}$ lower than the given $T_{\rm eff}$ for δ Scuti

[7] https://mast.stsci.edu

Table 1
The List of Candidate DSEBs and their Properties

TIC Number	R.A. (J2000)	Decl. (J2000)	P_{orb} (day)	V (mag)	T_{eff} (K) ± 181	$\log g$ ± 0.09	Sectors
8669966	$16^h33^m29^s.1$	$+30^\circ29'56''.6$	3.400272 (6)	6.89	7651	3.54	25
10057647	$08^h53^m19^s.3$	$+53^\circ44'08''.9$	16.259725 (5)	8.52	7249	4.06	20, 47
13037534[a]	$22^h55^m30^s.2$	$+64^\circ00'31''.0$	30.220888 (9)	11.29	5694	…	17, 18, 24
14948284	$12^h41^m07^s.8$	$+30^\circ26'13''.6$	2.699312 (8)	6.95	7178	3.86	22
48084398	$18^h47^m29^s.6$	$+49^\circ25'55''.3$	4.243430 (7)	7.20	6814	3.29	14, 15, 26, 40
71613490	$13^h29^m56^s.1$	$+34^\circ31'27''.4$	1.313542 (7)	7.69	7737	3.84	23
72839144[b]	$16^h56^m28^s.7$	$+37^\circ39'18''.9$	1.755764 (2)	10.03	7189	3.68	25
75593781[c]	$05^h41^m34^s.9$	$+25^\circ59'52''.9$	1.532149 (6)	11.39	8300	4.33	43, 44, 45
78148497	$05^h54^m24^s.5$	$+26^\circ18'31''.7$	2.708848 (5)	10.96	7287	3.93	43, 45
85600400	$17^h16^m49^s.9$	$+38^\circ21'58''.7$	1.471461 (5)	12.19	7235	3.85	25, 26
116334565	$05^h40^m28^s.4$	$+30^\circ58'27''.3$	3.475191 (7)	11.32	7546	3.60	43, 45
165618747	$17^h20^m07^s.8$	$+13^\circ39'57''.6$	0.648264 (3)	11.67	7603	4.11	25, 26
172431974	$19^h58^m50^s.1$	$+39^\circ19'52''.1$	2.387408 (3)	10.96	7236	3.71	14, 15, 41
193774939[d]	$17^h53^m12^s.7$	$+43^\circ46'23''.2$	1.305766 (7)	10.16	7358	4.05	25, 26
197755658[e]	$22^h28^m01^s.7$	$+53^\circ41'00''.1$	3.158785 (4)	11.46	7645	3.86	16,17
197757000[f]	$22^h28^m49^s.9$	$+53^\circ46'15''.9$	2.185923 (7)	11.10	6985	3.92	16, 17
240962482	$01^h15^m58^s.9$	$+52^\circ46'40''.0$	4.475000 (1)	10.12	7748	3.81	18
241013310	$01^h20^m12^s.8$	$+48^\circ36'41''.4$	2.144879 (6)	10.11	7093	4.01	17, 18
256640561	$21^h51^m35^s.4$	$+71^\circ53'08''.7$	1.712080 (2)	8.41	7891	3.48	17, 18, 24, 25
272822330	$23^h46^m17^s.9$	$+62^\circ01'33''.4$	4.501230 (4)	10.06	7340	3.56	17, 18, 24
289947843	$06^h40^m16^s.6$	$+79^\circ35'58''.3$	…	6.75	9175	4.12	19, 20, 26, 40, 47
301909087[g]	$02^h41^m16^s.5$	$+48^\circ56'18''.8$	4.448759 (6)	10.81	6847	3.54	18
305633328	$21^h02^m23^s.9$	$+60^\circ04'41''.9$	2.506158 (3)	11.76	6899	…	16, 17
322428763	$18^h35^m03^s.3$	$+28^\circ49'40''.1$	6.714251 (8)	11.18	6151	3.27	40
327121759[h]	$00^h13^m30^s.1$	$+58^\circ17'00''.8$	2.990910 (1)	11.67	7159	3.69	17, 18, 24
337094559	$22^h22^m32^s.6$	$+63^\circ35'10''.6$	1.777515 (8)	9.98	7424	3.72	24
338159479[i]	$22^h32^m15^s.5$	$+64^\circ58'40''.3$	1.414305 (1)	12.07	…	…	17, 18, 24
354926863	$02^h37^m46^s.2$	$+67^\circ51'19''.9$	1.436540 (3)	10.98	7388	4.07	18, 19, 25
358613523[j]	$11^h40^m24^s.7$	$+80^\circ14'09''.5$	1.327830 (5)	10.31	7271	4.28	14, 20, 21[n]
393894013[k]	$13^h13^m33^s.4$	$+47^\circ47'51''.9$	0.816127 (4)	9.34	7866	4.19	22
396134795	$23^h48^m23^s.6$	$+36^\circ18'40''.3$	2.586765 (4)	10.11	6946	3.80	17
396201681	$23^h58^m06^s.1$	$+67^\circ36'11''.4$	7.039790 (1)	10.16	7767	…	17, 18, 24, 25
420114772	$19^h21^m43^s.2$	$+74^\circ45'45''.5$	6.470060 (5)	10.47	7015	…	14–26, 41, 47
421714420	$21^h38^m45^s.8$	$+55^\circ47'29''.9$	…	7.90	8820	3.81	16,17
428003183	$23^h16^m53^s.1$	$+44^\circ29'18''.4$	0.742981 (7)	11.11	7345	4.05	16, 17
430808126	$22^h15^m58^s.4$	$+53^\circ18'43''.1$	6.481440 (7)	11.56	8460	…	16, 17
440003271[l]	$00^h10^m03^s.2$	$+46^\circ23'25''.1$	2.639210 (1)	7.51	8334	4.16	17
456905229[m]	$01^h44^m53^s.5$	$+19^\circ51'24''.5$	1.692620 (8)	8.44	7041	…	17, 42, 43
467354611	$21^h46^m23^s.5$	$+77^\circ22'19''.7$	…	9.76	6235	3.35	17, 19, 25, 26

Notes. The atmospheric parameters were taken from the TIC (Stassun et al. 2019) and an average error is stated for these parameters.
[a] F1V (Avvakumova et al. 2013).
[b] F0+G9 IV (Svechnikov & Kuznetsova 2004).
[c] B9 (Avvakumova et al. 2013).
[d] F1V+K6 (Avvakumova et al. 2013).
[e] A9.5V+F3.5V (Avvakumova et al. 2013).
[f] A5 (Avvakumova et al. 2013).
[g] A2+G6IV (Budding et al. 2004).
[h] A0(Avvakumova et al. 2013).
[i] A8+G8IV (Budding et al. 2004).
[j] A5+G6IV (Budding et al. 2004).
[k] A3 (Avvakumova et al. 2013).
[l] A3 (Avvakumova et al. 2013).
[m] F0 (Avvakumova et al. 2013).
[n] 14, 20, 21, 26, 40, 41.

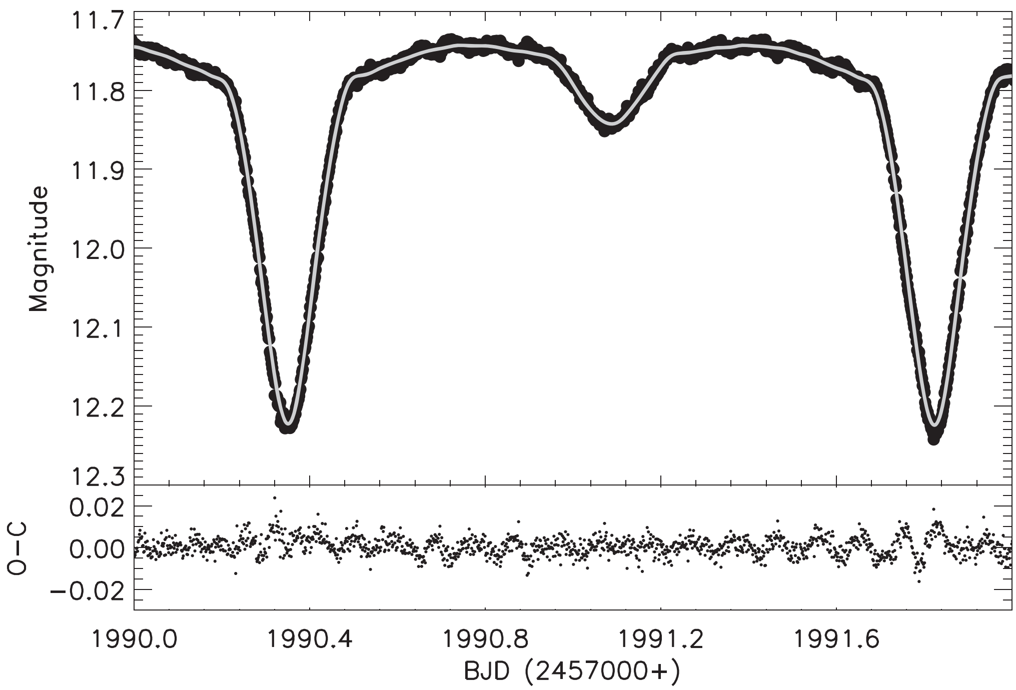

Figure 1. Top: The fit (gray line) of the orbital frequency and its harmonics to the TESS data of TIC 85600400. Bottom: Residuals.

stars even considering a possible error. However, the target illustrates significant δ Scuti-type variations and its spectral type is identified as F1V in the catalog of Avvakumova et al. (2013). Considering a possible error in $T_{\rm eff}$, we included this target in our list as well. As a result, we have 39 candidates of DSEBs listed in Table 1.

For the analysis of the candidate DSEBs, we preferred to use only SC data because the Nyquist frequency for the SC data reaches ~360 day^{-1}. Taking into account the typical frequency range of δ Scuti variables (~4−80 day^{-1}, Aerts et al. 2010), the SC data are the most suitable data for an examination of δ Scuti-type variations. In Table 1, the available TESS sectors for each target are listed. The SAP and PDCSAP fluxes of our targets were controlled and they were found to be similar. As the PDCSAP fluxes are the fluxes with long term trends removed and mostly cleaner data, we preferred to use the PDCSAP fluxes. Each of the fluxes was converted into magnitude[8] to use in the analysis.

3. Frequency Analysis

In the current study, our main goal is revealing δ Scuti-type variations in our candidate systems. Therefore, we carried out a frequency analysis for each system. We used the PERIOD04 program which derives individual frequencies from astronomical data including gaps and also allows us to find the combination and harmonic frequencies (Lenz & Breger 2005). Our analysis consists of two steps. In the first step, the binary variations were removed from all available data of each target to obtain only the variation of oscillations. The binary variations were removed from the data with a phenomenological fit including the frequency of orbital periods and their harmonics (Kahraman Aliçavuş et al. 2022). Before starting this analysis, the orbital periods of each target were calculated by performing a frequency analysis and these orbital periods were used in the current research. We could not determine the orbital periods for some systems because there is only one primary eclipse in their data. The derived orbital parameters are given in Table 1. In Figure 1, we show one example of orbital period frequency fits to the TESS data and the residuals. As can clearly be seen from the figure, the binary variations were extracted and only the light curve of the pulsations was obtained. In the light curves of some systems, there are only one or two eclipses in available data. For these systems, no orbital frequency fit was applied, and only the eclipse(s) was removed from the light curves and the rest was analyzed.

After the binary variations were removed from the TESS data of all targets, we carried out a frequency analysis of the residuals in the second step of the analysis. The independent, harmonic and combination frequencies were searched for. During the analysis, the frequencies having a signal-to-noise ratio (S/N) over 4.5 were expected to be significant. A typical significance limit for the detected frequencies is given as 4.0 by Breger et al. (1993). However, Baran & Koen (2021) showed that this limit should be higher for TESS data and by taking

[8] Flux [e^{-} s^{-1}] = 10 $^{(20.44-{\rm TESS_{mag}}/2.5)}$.

Table 2
Calculated Physical Parameters, *I* Ratios of the Binary Components and the Range and Number of Detected Frequencies

TIC Number	A_v (mag) $\pm$ 0.002	M_V (mag)	$M_{\rm bol}$ (mag)	log $(L/L_\odot)$	I_p/I_s $\pm$ 0.10	Frequency range (day^{-1})	Number of frequencies
8669966	0.031	0.716 ± 0.025	0.767 ± 0.025	1.610 ± 0.045	1.23	13.103–14.21	6
10057647	0.192	2.164 ± 0.032	2.237 ± 0.032	1.030 ± 0.052	1.40	13.77–51.41	23
13037534	0.720	0.571 ± 0.025	0.588 ± 0.024	1.668 ± 0.045	6.64	8.84–12.11	8
14948284	0.069	1.807 ± 0.024	1.883 ± 0.029	1.173 ± 0.044	1.20	8.09–24.92	21
48084398	0.048	0.555 ± 0.029	0.635 ± 0.032	1.674 ± 0.049	1.04	8.98–13.22	21
71613490	0.029	1.395 ± 0.032	1.441 ± 0.007	1.338 ± 0.052	1.04	24.47–32.34	19
72839144	0.077	1.416 ± 0.007	1.492 ± 0.028	1.329 ± 0.027	3.55	4.11	1
75593781	0.708	1.364 ± 0.029	1.355 ± 0.016	1.350 ± 0.049	4.47	46.11–57.94	15
78148497	0.663	1.324 ± 0.016	1.395 ± 0.032	1.367 ± 0.036	2.80	9.77–32.97	22
85600400	0.087	1.651 ± 0.032	1.724 ± 0.027	1.236 ± 0.052	3.85	9.70–19.97	17
116334565	0.809	0.849 ± 0.027	0.908 ± 0.031	1.557 ± 0.047	1.27	6.55–22.85	12
165618747	0.298	2.107 ± 0.031	2.162 ± 0.011	1.053 ± 0.051	1.97	15.13–40.18	28
172431974	0.047	1.557 ± 0.011	1.631 ± 0.032	1.273 ± 0.031	1.01	4.24–6.40	10
193774939	0.080	2.220 ± 0.033	4.974 ± 0.019	1.008 ± 0.053	5.16	16.59–31.21	21
197755658	0.029	2.074 ± 0.019	2.126 ± 0.013	1.066 ± 0.039	1.94	46.63–51.26	3
197757000	0.123	2.576 ± 0.013	2.657 ± 0.009	0.865 ± 0.033	4.46	21.17–41.98	21
240962482	0.190	1.689 ± 0.010	1.733 ± 0.007	1.221 ± 0.030	11.84	24.96–29.43	5
241013310	0.110	2.335 ± 0.007	2.414 ± 0.033	0.962 ± 0.027	4.02	4.82–14.77	4
256640561	0.079	0.823 ± 0.033	0.855 ± 0.007	1.567 ± 0.053	1.86	10.12–24.42	12
272822330	0.165	0.997 ± 0.007	1.066 ± 0.030	1.497 ± 0.027	1.91	14.03–20.34	11
289947843	0.083	0.912 ± 0.030	0.791 ± 0.012	1.531 ± 0.050	…	5.97–14.44	11
301909087	0.624	1.137 ± 0.012	1.218 ± 0.026	1.441 ± 0.032	1.04	5.58–17.44	10
305633328	0.245	1.680 ± 0.026	1.760 ± 0.014	1.224 ± 0.046	1.08	9.38–15.37	8
322428763	0.174	1.441 ± 0.014	1.517 ± 0.022	1.483 ± 0.014	1.53	11.99–49.78	11
327121759	0.726	1.374 ± 0.022	1.451 ± 0.011	1.346 ± 0.042	3.43	22.90–30.97	6
337094559	0.097	2.049 ± 0.011	2.114 ± 0.061	1.077 ± 0.031	1.78	7.86–19.47	8
338159479	0.292	2.332 ± 0.062	2.383 ± 0.011	0.963 ± 0.081	2.01	21.75–28.51	17
354926863	0.298	2.755 ± 0.011	2.822 ± 0.007	0.794 ± 0.031	1.06	4.66–39.11	18
358613523	0.097	2.813 ± 0.007	2.885 ± 0.034	0.771 ± 0.027	5.16	24.59–46.44	15
393894013	0.044	2.216 ± 0.035	2.250 ± 0.023	1.010 ± 0.055	1.49	8.55–69.65	19
396134795	0.628	1.290 ± 0.023	1.371 ± 0.038	1.380 ± 0.043	1.63	14.20–28.47	7
396201681	0.184	1.595 ± 0.038	1.638 ± 0.071	1.258 ± 0.058	1.14	1.21–23.52	11
420114772	0.127	0.656 ± 0.071	0.736 ± 0.016	1.634 ± 0.091	1.05	5.02–41.95	30
421714420	0.097	-0.083 ± 0.016	-0.154 ± 0.014	1.929 ± 0.036	10.00	4.01–53.19	11
428003183	0.106	2.438 ± 0.014	2.506 ± 0.015	0.921 ± 0.034	2.56	12.93–32.77	22
430808126	…	…	…	…	1.07	5.26–27.63	22
440003271	0.030	1.524 ± 0.026	1.510 ± 0.026	1.287 ± 0.046	1.10	12.19–37.33	19
456905229	0.048	2.060 ± 0.074	2.139 ± 0.074	1.072 ± 0.094	1.12	10.13–33.39	44
467354611	0.094	1.825 ± 0.023	1.166 ± 0.043	1.876 ± 0.027	…	11.58–31.04	41

Note. For TIC 430808126, parameters could not be calculated as it has no parallax.

into account the results obtained in their study, we took the significance limit as 4.5. The analysis was carried out for a range of $\sim$4–80 day^{-1} considering the typical pulsation period of δ Scuti stars (see Section 1). Two objects in our targets (TIC 396201681, TIC 421714420) clearly display long-term variations that could be a γ Doradus-type oscillation. Therefore for these systems, the frequency analysis was performed for the $\sim$0–80 day^{-1} range of frequency, as γ Doradus stars typically exhibit pulsations with a frequency changing from $\sim$0.3 to 3 day^{-1} (Aerts et al. 2010). Consequently, the range and number of detected frequencies are listed in Table 2. The first five highest amplitude frequencies are also expressed in Table 4 for each target. The full table is given in electronic form. The frequency spectrum and the fits of the calculated frequencies to the observations are depicted in Figure 2 for one sample and in Figure 5 for the others.

4. Calculating Physical Parameters

For all systems, we calculated some physical parameters such as luminosity (L), absolute (M_V) and bolometric ($M_{\rm bol}$) magnitudes. However, one should keep in mind that these parameters represent the binary system and do not belong to only one binary component. Before starting to calculate these parameters, we estimated flux densities of binary components to estimate the flux contributions of each component to the total. It is known that the area ratio of eclipses approximately gives the flux density ratio of the binary components (Binnendijk 1960). In the primary eclipse (deeper one), the loss of light is more than the secondary eclipse, so in the primary eclipse, the star with the higher surface luminosity, and hence hotter, is obscured by the other. We call this star the primary (p) and the other cool and less luminous one the secondary (s) component. The areas of the primary (A_p) and secondary (A_s) eclipses were measured by using the IRAF[9] (Tody 1986) splot task. The ratio of these areas is equal to flux density (I) ratio as shown in the following equation (Binnendijk 1960)

$$\frac{A_p}{A_s} = \frac{I_p}{I_s}. \tag{1}$$

The calculated I ratios are listed in Table 2. For some systems, there is only one eclipse available in the light curves, therefore flux ratio value could not be determined for these systems. As can be seen from the I ratios, in most systems, I values of the primary and secondary components are close to each other. We assume that if the I ratio is over ∼4 the calculated physical parameters mostly belong to the primary component.

The physical parameters of all systems were calculated using the distance modulus and the Pogson equation. To compute these parameters, the distances of the systems were taken from the Gaia Early Data Release 3 (EDR3, Gaia Collaboration et al. 2021) and also extinction coefficient (A_v) was calculated utilizing the interstellar extinction maps of Amôres & Lépine (2005). First the M_V parameters were calculated with the following equation

$$V - M_V = 5\log d - 5 + A_v, \tag{2}$$

where V is the visual magnitude and d is the distance of the systems. After the M_V values were derived, the $M_{\rm bol}$ parameters were computed taking into account the TIC $T_{\rm eff}$ values and bolometric corrections from Eker et al. (2020). If there is no $T_{\rm eff}$ value for a system, we estimated this value from the target's spectral type by considering the calibration between the spectral type and $T_{\rm eff}$ given by Gray (1992). Additionally, for TIC 13037534, $T_{\rm eff}$ determined from the spectral type-$T_{\rm eff}$ calibration was used. Then, the L parameters were computed with the following equation

$$\frac{L}{L_\odot} = 10^{(M_{\rm bol\odot} - M_{\rm bol})/2.5}. \tag{3}$$

The $M_{\rm bol\odot}$ value is taken as $4\overset{\rm m}{.}74$ according to IAU 2015 General Assembly Resolution B2.[10] The calculated parameters are given in Table 2. Uncertainties of the computed parameters are estimated considering the errors in the input parameters. According to the I ratio of the primary and secondary components, these calculated parameters mostly represent the binary systems. However, there are some systems in which the given I ratio is over ∼4. In these systems the flux coming from the primary is significantly higher than that from the secondary and we assume the calculated physical parameters mostly represent the hotter primary component and probably the pulsating one.

5. Discussion

In this section, we examine some properties of our candidate DSEBs.

5.1. Pulsation Type

In this study, we present the analysis of some targets showing δ Scuti like variations. While determining the candidate DSEBs, one of the important criteria was the $T_{\rm eff}$ of the eclipsing binary systems. However, we know that these $T_{\rm eff}$ values are an average of both binary components. So, real $T_{\rm eff}$ of pulsating components could be higher or cooler than the TIC $T_{\rm eff}$. In some systems, we found that the primary components have significantly more flux density compared to the secondaries (see Table 2). In these systems,[11] the $T_{\rm eff}$ mostly represents the hotter primary and probably the pulsating component. When we examined the $T_{\rm eff}$ values[12] of these systems, we found that their $T_{\rm eff}$ values are in the range of the $T_{\rm eff}$ given for δ Scuti stars. Their pulsation amplitudes and frequencies are also consistent with the values published for δ Scuti stars (Aerts et al. 2010).

For the other systems which have the I ratio lower than 4, probably the TIC $T_{\rm eff}$ values are substantially different from the real $T_{\rm eff}$ values of the pulsating components. Inside the pulsating stars, there are two different types that exhibit frequencies like δ Scuti variables. One of them is β Cephei stars. The β Cephei stars mostly manifest frequencies between 3 and 12 day^{-1} and these pulsators have B0–B3 spectral type (Aerts et al. 2010). Although these pulsators are quite hotter than the δ Scuti variables, if a β Cephei star has a very cool binary component, the total $T_{\rm eff}$ of the system will be cooler than the value expected for the β Cephei stars. However, our targets have a $T_{\rm eff}$ value in the range of ∼6300–9100 K and even if a β Cephei star has a cool binary component, the average $T_{\rm eff}$ of the binary system could not be as low as our targets' $T_{\rm eff}$ range.

Another pulsating star group is the Maia variables. The existence of Maia variables has not been exactly confirmed, however, for decades Maia variables have been considered as a new group of pulsating stars (Aerts & Kolenberg 2005; Balona et al. 2016; Balona & Ozuyar 2020). The Maia variables are

[9] http://iraf.noao.edu/

[10] https://www.iau.org/static/resolutions/IAU2015_English.pdf

[11] TIC 13037534, TIC 75593781, TIC 85600400, TIC 193774939, TIC 197757000, TIC 240962482, TIC 241013310, TIC 358613523 and TIC 421714420.

[12] For TIC 13037534, the spectral type was taken into account.

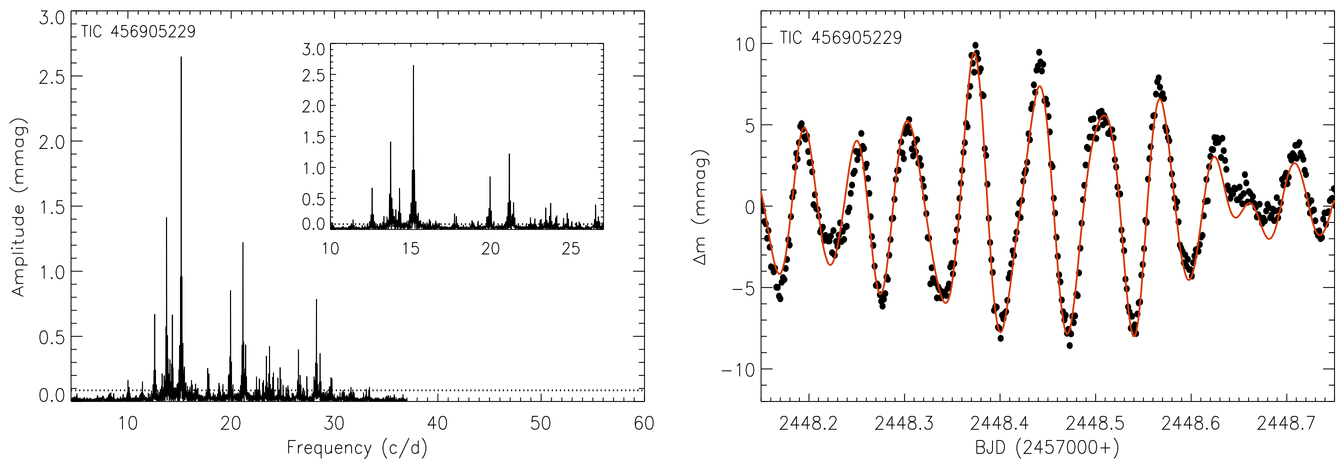

Figure 2. Left: The frequency spectrum of TIC 456905229. The dashed line represents the 4.5σ level. Right: Theoretical fit (red solid line) to observed data (dots) for TIC 456905229.

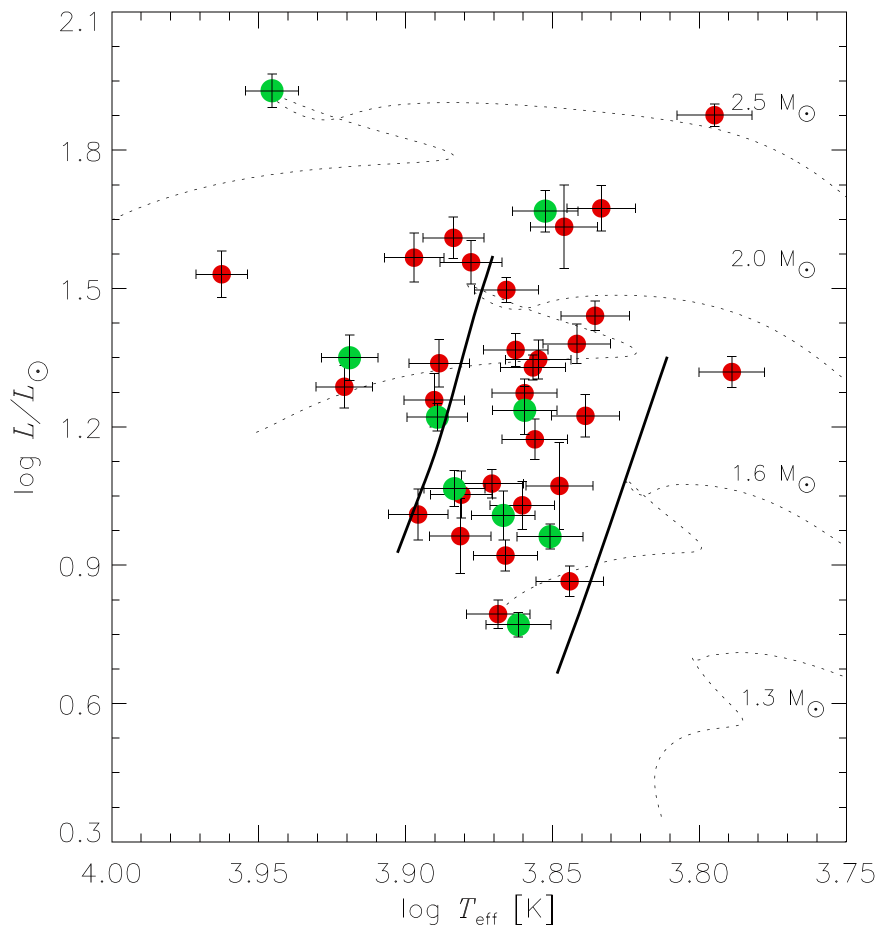

Figure 3. Positions of the targets in the H-R diagram. Green dots represent the systems having *I* ratio higher than ∼4, while red smaller dots signify the other systems. The solid and dashed lines are the borders of the δ Scuti instability strip (Dupret et al. 2005) and the evolutionary tracks taken from the MESA Isochrones and Stellar Tracks (MIST) (Paxton et al. 2011; Choi et al. 2016; Dotter 2016), respectively.

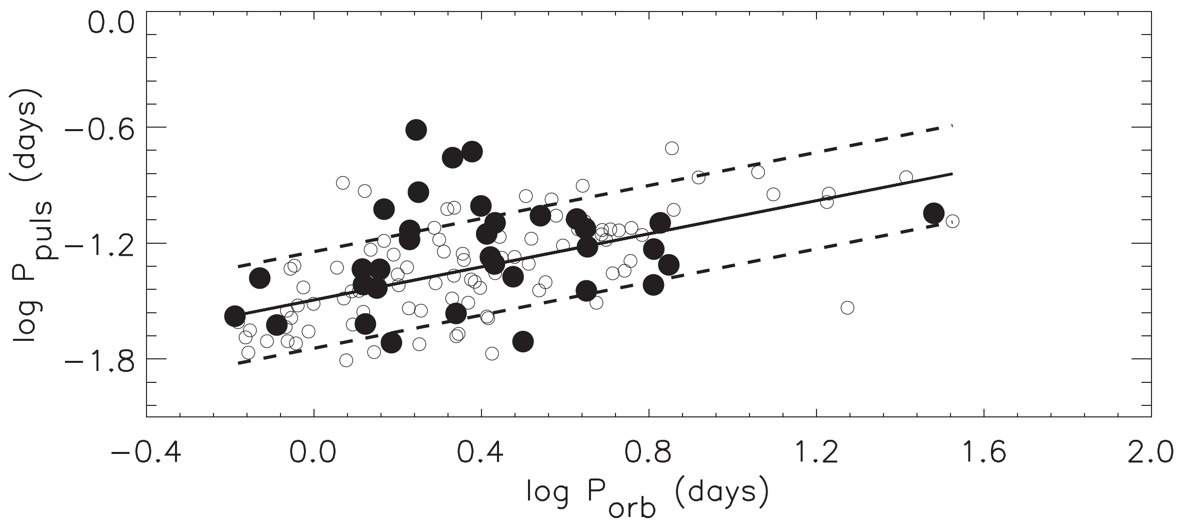

Figure 4. Consistency of the candidate DSEBs with the P_{orb}–P_{puls} relationship. The filled and empty circles represent our candidate and the known DSEBs (Kahraman Aliçavuş et al. 2017), respectively. The solid and dashed lines correspond to the correlation and 1σ level, respectively.

located between the β Cephei and δ Scuti stars, so they are cooler than β Cephei variables and hotter than the δ Scuti stars. Additionally, Maia variables demonstrate oscillations approximately in a similar frequency range with the δ Scuti stars (Balona et al. 2016; Balona & Ozuyar 2020). Even the existence of Maia variables has not been confirmed, and even if they are a new type of variable, they could be a member of binary systems and appear cooler than expected if a Maia variable has a cooler binary component. In this case, they could be considered as a δ Scuti variable. To have an idea about the variability type of our targets, their positions in the Hertzsprung–Russell (H-R) diagram should be examined by considering the I ratios. Therefore, we show the positions of our systems in the H-R diagram by using the parameters expressed in Tables 1 and 2.

As can be seen from Figure 3, most of the systems, which have an I ratio over around 4, are located in the δ Scuti instability strip and for these systems, we assume the L and T_{eff} mostly represent the primary, probably the pulsating, binary component. Inside these systems, there is one object (TIC 421714420) that is placed beyond the hot border of the δ Scuti instability strip. In a detailed study of the Kepler field focusing on δ Scuti and related stars, Uytterhoeven et al. (2011) reported that there are some real δ Scuti variables located beyond the borders of the δ Scuti instability strip. However, this system is noticeable far from the δ Scuti instability strip, and very close to the place where Maia variables are located (Balona & Ozuyar 2020). Therefore we classified this system as a candidate Maia variable in an eclipsing binary. There is another system located beyond the hotter border of δ Scuti stars, TIC 289947843, unfortunately, we could not measure the I ratio for this system because there are not enough data. For the other systems having I ratio <4, the L value of the pulsating component should be lower than the calculated one and depending on T_{eff} of the other binary component, the T_{eff} of the pulsating star could be lower or higher than that used in the H-R diagram. Taking into account these conditions, we could say that most pulsating components could be located inside the δ Scuti instability strip, however it is difficult to have an idea about the variability of the systems considering this. Therefore, as a result of this examination, we classified 38 systems as candidate DSEBs and one of them, TIC 421714420, as a Maia candidate in an eclipsing binary system.

5.2. Consistency with the Known Relationship for DSEBs

DSEBs have been investigated for a long time and it was shown that there are some relationships between the pulsation period, amplitude and other parameters such as P_{orb}, R and $\log g$ (Kahraman Aliçavuş et al. 2017; Liakos & Niarchos 2017). For DSEBs, the well-known relationship is between the P_{orb} and P_{puls}. In the latest study of Kahraman Aliçavuş et al. (2017), it was demonstrated that known DSEBs obey this relationship within error bars. We examined whether our candidate systems obey this relationship. In this section, we only investigate the candidate DSEBs. As can be seen from Figure 4, most of our candidates are consistent with the relationship within errors. There are a few objects significantly located outside of the 1σ level, TIC 72839144, TIC 172431974, TIC 197755658 and TIC 241013310. The reason for these could be the additional effect in the binary system such as mass transfer between binary components if these systems are DSEBs.

Table 3
Calculated Parameters from the Given Relationships by Kahraman Aliçavuş et al. (2017)

TIC Number	$\log g$ (cgs)	R ($R_\odot$)	M ($M_\odot$)
8669966	3.65 ± 0.20	3.53 ± 0.39	2.07 ± 0.30
10057647	4.41 ± 0.24	1.39 ± 0.24	1.85 ± 0.38
13037534	3.51 ± 0.28	3.93 ± 0.51	1.85 ± 0.40
14948284	3.93 ± 0.10	2.74 ± 0.32	2.38 ± 0.10
48084398	3.56 ± 0.26	3.80 ± 0.47	1.93 ± 0.36
71613490	4.10 ± 0.11	2.25 ± 0.05	2.39 ± 0.06
75593781	4.59 ± 0.34	0.88 ± 0.39	1.13 ± 0.36
78148497	3.59 ± 0.24	3.70 ± 0.44	1.98 ± 0.34
116334565	3.53 ± 0.28	3.87 ± 0.49	1.88 ± 0.38
165618747	4.37 ± 0.22	1.52 ± 0.20	1.97 ± 0.34
193774939	3.97 ± 0.12	2.62 ± 0.12	2.40 ± 0.19
197757000	4.35 ± 0.20	1.57 ± 0.18	2.03 ± 0.30
240962482	4.16 ± 0.14	2.10 ± 0.03	2.36 ± 0.09
256640561	3.44 ± 0.32	4.11 ± 0.56	1.75 ± 0.44
272822330	3.79 ± 0.12	3.14 ± 0.28	2.25 ± 0.20
289947843	3.69 ± 0.18	3.41 ± 0.36	2.13 ± 0.28
301909087	3.64 ± 0.22	3.57 ± 0.40	2.05 ± 0.32
305633328	3.45 ± 0.32	4.10 ± 0.56	1.75 ± 0.44
322428763	3.59 ± 0.24	3.70 ± 0.44	1.98 ± 0.34
327121759	4.04 ± 0.10	2.44 ± 0.17	2.41 ± 0.22
338159479	4.13 ± 0.10	2.17 ± 0.01	2.38 ± 0.09
354926863	3.98 ± 0.10	2.61 ± 0.12	2.40 ± 0.17
358613523	4.43 ± 0.26	1.32 ± 0.26	1.77 ± 0.42
393894013	4.44 ± 0.26	1.30 ± 0.26	1.74 ± 0.44
396134795	3.68 ± 0.10	3.44 ± 0.37	2.11 ± 0.28
396201681	3.94 ± 0.10	2.72 ± 0.15	2.38 ± 0.17
420114772	4.11 ± 0.10	2.24 ± 0.05	2.39 ± 0.07
421714420	4.27 ± 0.16	1.78 ± 0.24	2.20 ± 0.22
428003183	4.05 ± 0.10	2.40 ± 0.06	2.41 ± 0.11
430808126	3.81 ± 0.06	3.09 ± 0.26	2.27 ± 0.18
440003271	3.87 ± 0.14	2.90 ± 0.21	2.34 ± 0.14
456905229	3.73 ± 0.16	3.31 ± 0.33	2.18 ± 0.24
467354611	3.71 ± 0.16	3.35 ± 0.34	2.16 ± 0.26

More relationships between the $P_{\rm puls}$ and other parameters are described by Kahraman Aliçavuş et al. (2017) for detached and semi-detached systems. These parameters help us approximately estimate some physical parameters of the δ Scuti pulsating components in eclipsing binary systems. As we do not know the Roche geometry of our systems, we could not classify the binary configurations of our targets. However, for both detached and semi-detached binary configurations, some relationships yield a good correlation between the $P_{\rm puls}$ such as $\log g$ and the radius (R) of the pulsating component. Therefore, we calculated $\log g$ and R parameters of our systems using the equations given in the study of Kahraman Aliçavuş et al. (2017). In this calculation, we excluded the systems found outside of the $P_{\rm orb}$–$P_{\rm puls}$ relationship. The computed $\log g$ and R parameters are listed in Table 3. By utilizing the calculated $\log g$ and R, we also estimated the mass (M) values of the pulsating component. These values are also listed in Table 3. It should be kept in mind that these parameters are just an estimation and do not give exact values and the real errors should be higher.

6. Conclusions

In this study, we present the results of our northern TESS field search to discover new eclipsing binaries with δ Scuti components. We first determined 39 targets and examined the pulsational properties (pulsation amplitude and frequencies) of these systems after removing the eclipsing variations. In addition to determining pulsation amplitude and frequencies, we also estimated the l ratios of binary components to find how much binary components contribute to total flux relative to each other. To estimate whether our systems could be DSEBs or not, we also controlled the positions of the targets in the H-R diagram. For this, we calculated the L parameters of the systems. By considering the positions of the systems in the H-R diagram and the l ratios, we showed that one of our targets (TIC 421714420) could be a candidate Maia variable in an eclipsing binary system. The other targets in the study are classified as candidate DSEBs. However, to be sure about the positions of the systems in the H-R diagram and their real $T_{\rm eff}$ values, detailed spectroscopic analysis and binary modeling are necessary. With the spectroscopy, the $T_{\rm eff}$ value of each binary component could be derived and with the binary modeling, the real L parameters could be reached.

We know that the pulsating eclipsing binary systems are quite important for deeply understanding stellar systems. An increasing number of these kinds of systems would contribute to improving our knowledge about stellar evolution and structure. Therefore, this study would be useful for both probing stellar structure and evolution, and understanding the pulsation behavior of oscillating stars in eclipsing binary systems.

Acknowledgments

This work has been supported in part by the Scientific and Technological Research Council (TUBITAK) under Grant No. 120F330. The TESS data presented in this paper were obtained from the Mikulski Archive for Space Telescopes (MAST). F.K.A. thanks Prof. Gerald Handler for showing how to clean binarity with a phenomenological fit. Funding for the TESS mission is provided by the NASA Explorer Program. This work has made use of data from the European Space Agency (ESA) mission Gaia (http://www.cosmos.esa.int/gaia), processed by the Gaia Data Processing and Analysis Consortium (DPAC, http://www.cosmos.esa.int/web/gaia/dpac/consortium). Funding for the DPAC has been provided by national institutions, in particular the institutions participating in the Gaia Multilateral Agreement. This research has made use of the SIMBAD database, operated at CDS, Strasbourq, France.

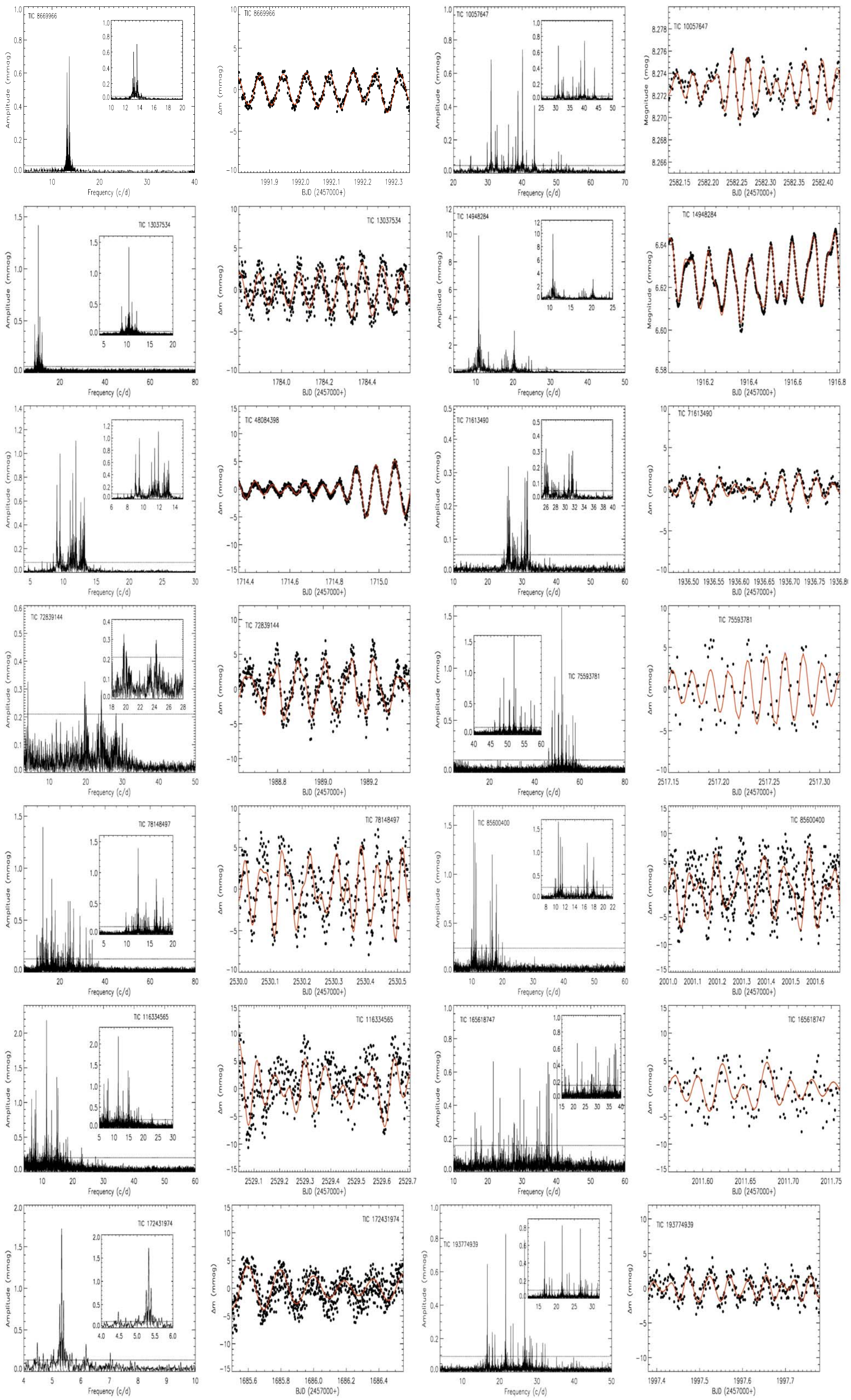

Figure 5. Amplitude spectra of the targets and the theoretical frequency fit (red solid lines) to the observations. Dotted lines represent the 4.5σ level.

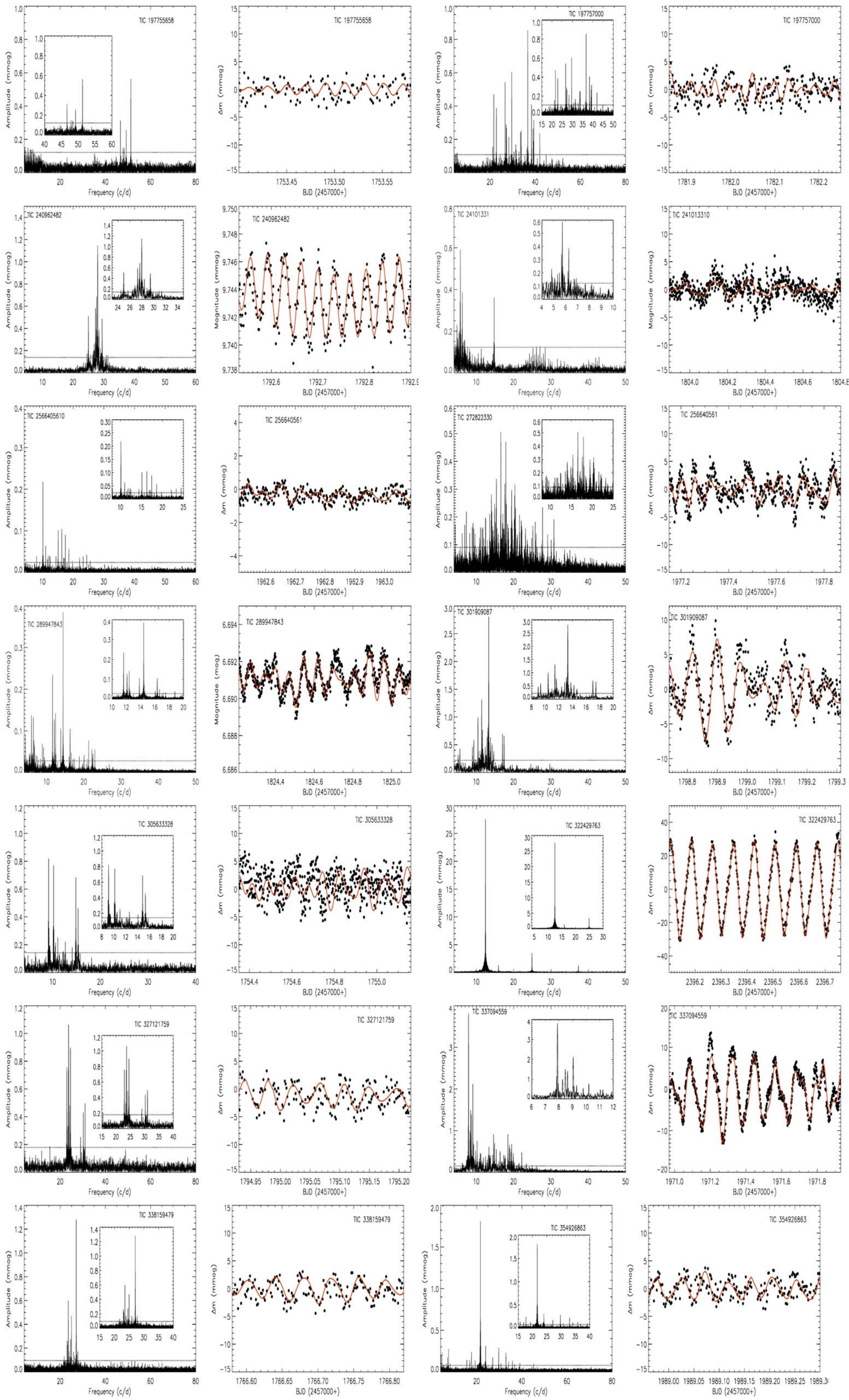

Figure 5. (Continued.)

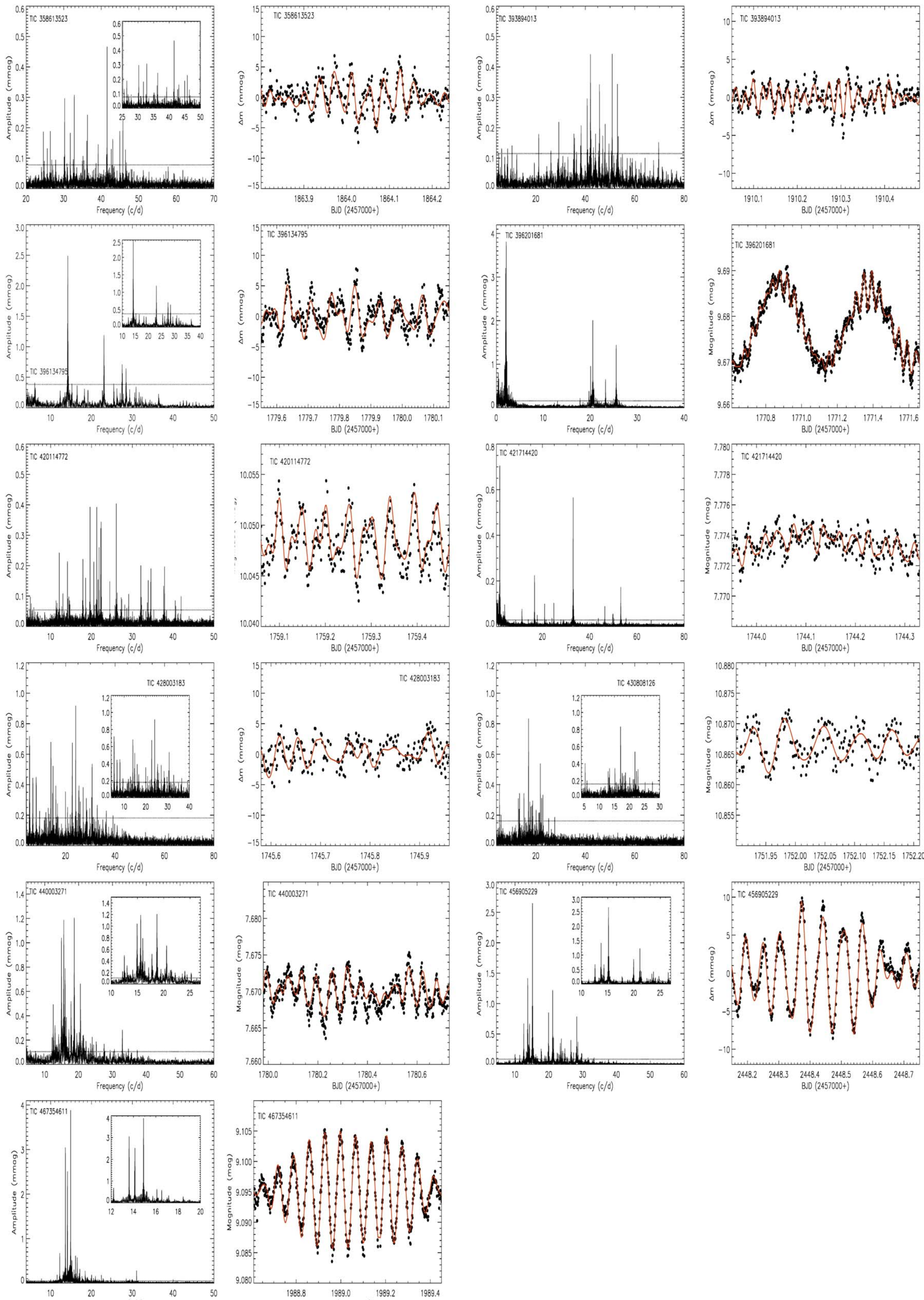

Figure 5. (Continued.)

Table 4
The List of the First Five Highest Amplitude Frequencies Detected in this Study

	Frequency (day^{-1})	Amplitude (mmag)	Phase (rad)	S/N		Frequency (day^{-1})	Amplitude (mmag)	Phase (rad)	S/N		Frequency (day^{-1})	Amplitude (mmag)	Phase (rad)	S/N
	TIC 8669966					TIC 10057647					TIC 13037534			
ν_1	13.62189 ± 0.00015	0.717 ± 0.005	0.5562 ± 0.0011	62	ν_1	40.11281 ± 0.00019	0.727 ± 0.007	0.2288 ± 0.0015	54	ν_1	11.10889 ± 0.00004	0.526 ± 0.012	0.8332 ± 0.0036	20
ν_2	13.14363 ± 0.00017	0.618 ± 0.005	0.0358 ± 0.0013	61	ν_2	30.95924 ± 0.00020	0.686 ± 0.007	0.1324 ± 0.0015	69	ν_2	8.84272 ± 0.00006	0.459 ± 0.012	0.3634 ± 0.0048	24
ν_3	13.32788 ± 0.00038	0.278 ± 0.005	0.0784 ± 0.0028	26	ν_3	38.78309 ± 0.00028	0.481 ± 0.007	0.8545 ± 0.0022	31	ν_3	9.74327 ± 0.00006	0.323 ± 0.012	0.4381 ± 0.0055	13
ν_4	13.03191 ± 0.00042	0.251 ± 0.005	0.0809 ± 0.0031	25	ν_4	36.01630 ± 0.00048	0.283 ± 0.007	0.6612 ± 0.0037	28	ν_4	10.63240 ± 0.00015	0.210 ± 0.012	0.2293 ± 0.0045	8
ν_5	13.73165 ± 0.00049	0.217 ± 0.005	0.5787 ± 0.0036	19	ν_5	32.21150 ± 0.00051	0.265 ± 0.007	0.2457 ± 0.0040	28	ν_5	10.41897 ± 0.00026	0.207 ± 0.019	0.8755 ± 0.0495	8
	TIC 14948284					TIC 48084398					TIC 71613490			
ν_1	20.31697 ± 0.00019	3.130 ± 0.028	0.7751 ± 0.0014	22	ν_1	11.88739 ± 0.00006	1.099 ± 0.006	0.5054 ± 0.0008	30	ν_1	25.98838 ± 0.00049	0.323 ± 0.007	0.9887 ± 0.0035	24
ν_2	11.20278 ± 0.00021	2.776 ± 0.028	0.1298 ± 0.0016	20	ν_2	9.49467 ± 0.00006	1.009 ± 0.006	0.9585 ± 0.0009	24	ν_2	31.57531 ± 0.00054	0.289 ± 0.007	0.8029 ± 0.0039	26
ν_3	20.11472 ± 0.00038	1.567 ± 0.028	0.5509 ± 0.0029	11	ν_3	11.41491 ± 0.00007	0.861 ± 0.006	0.9264 ± 0.0010	25	ν_3	30.81604 ± 0.00057	0.274 ± 0.007	0.2540 ± 0.0041	23
ν_4	18.05449 ± 0.00038	1.541 ± 0.028	0.0802 ± 0.0029	16	$\nu_2+\nu_3$-ν_1	9.02219 ± 0.00008	0.784 ± 0.006	0.3972 ± 0.0011	19	ν_4	31.33778 ± 0.00061	0.257 ± 0.007	0.7478 ± 0.0043	22
ν_5	17.67646 ± 0.00048	1.247 ± 0.028	0.1414 ± 0.0036	14	ν_5	11.02949 ± 0.00010	0.632 ± 0.006	0.1951 ± 0.0014	18	ν_5	26.25839 ± 0.00065	0.242 ± 0.007	0.9569 ± 0.0046	15
	TIC 72839144					TIC 75593781					TIC 78148497			
ν_1	4.11102 ± 0.00133	0.328 ± 0.020	0.8042 ± 0.0098	6	ν_1	51.91704 ± 0.00011	1.544 ± 0.023	0.1718 ± 0.0024	46	ν_1	12.44590 ± 0.00009	1.383 ± 0.017	0.3311 ± 0.0020	39
ν_2	24.253 43 ± 0.00147	0.296 ± 0.020	0.0052 ± 0.0109	5	ν_2	48.85966 ± 0.00018	0.914 ± 0.023	0.8996 ± 0.0040	30	ν_2	16.39778 ± 0.00014	0.900 ± 0.017	0.5090 ± 0.0031	19
ν_3	19.70960 ± 0.00148	0.295 ± 0.020	0.4652 ± 0.0109	5	ν_3	52.40034 ± 0.00022	0.754 ± 0.023	0.5367 ± 0.0048	22	ν_3	23.67636 ± 0.00018	0.677 ± 0.017	0.9442 ± 0.0041	16
					ν_4	47.75704 ± 0.00028	0.588 ± 0.023	0.1146 ± 0.0062	20	ν_4	24.48400 ± 0.00019	0.662 ± 0.017	0.2477 ± 0.0042	16
					ν_5	50.61103 ± 0.00026	0.622 ± 0.023	0.7971 ± 0.0058	19	ν_5	26.07247 ± 0.00020	0.616 ± 0.017	0.5684 ± 0.0045	17
	TIC 85600400					TIC 116334565					TIC 165618747			
ν_1	10.57549 ± 0.00018	1.666 ± 0.027	0.6049 ± 0.0026	29	ν_1	11.42838 ± 0.00007	2.212 ± 0.117	0.4961 ± 0.0005	36	ν_1	37.87282 ± 0.00039	0.765 ± 0.025	0.5868 ± 0.0060	23
ν_2	11.01141 ± 0.00021	1.386 ± 0.027	0.2475 ± 0.0031	24	ν_2	14.76193 ± 0.00007	1.360 ± 0.117	0.8032 ± 0.0005	20	ν_2	37.54370 ± 0.00039	0.675 ± 0.025	0.4108 ± 0.0059	20
ν_3	11.39975 ± 0.00025	1.183 ± 0.027	0.8613 ± 0.0037	22	ν_3	7.97122 ± 0.00010	1.212 ± 0.117	0.7470 ± 0.0007	17	ν_3	35.11748 ± 0.00060	0.474 ± 0.025	0.1010 ± 0.0090	14
ν_4	16.63944 ± 0.00025	1.171 ± 0.027	0.3368 ± 0.0037	20	ν_4	15.15892 ± 0.00008	1.207 ± 0.117	0.7195 ± 0.0006	17	ν_4	23.54175 ± 0.00056	0.430 ± 0.025	0.9865 ± 0.0084	14
ν_5	17.99572 ± 0.00030	0.971 ± 0.027	0.3860 ± 0.0045	22	ν_5	6.54611 ± 0.00012	1.073 ± 0.117	0.7175 ± 0.0008	13	ν_5	30.49806 ± 0.00069	0.414 ± 0.025	0.6068 ± 0.0103	12
ν_1	5.32323 ± 0.00015	1.854 ± 0.026	0.3324 ± 0.0022	42	ν_1	21.59652 ± 0.00014	0.825 ± 0.010	0.6836 ± 0.0020	38	ν_1	51.25620 ± 0.00044	0.562 ± 0.024	0.9177 ± 0.0067	22
ν_2	4.27899 ± 0.00053	0.528 ± 0.026	0.5921 ± 0.0078	10	ν_2	26.67014 ± 0.00014	0.783 ± 0.010	0.7211 ± 0.0021	45	ν_2	46.63643 ± 0.00080	0.310 ± 0.024	0.7649 ± 0.0121	11
ν_3	4.24755 ± 0.00058	0.489 ± 0.026	0.7757 ± 0.0085	10	ν_3	16.69181 ± 0.00017	0.642 ± 0.010	0.9187 ± 0.0026	42	ν_3	49.19415 ± 0.00097	0.256 ± 0.024	0.7373 ± 0.0147	8
ν_4	5.12970 ± 0.00064	0.443 ± 0.026	0.6626 ± 0.0093	7	ν_4	23.58869 ± 0.00039	0.290 ± 0.010	0.2894 ± 0.0058	17					
ν_5	4.69256 ± 0.00079	0.356 ± 0.026	0.4970 ± 0.0116	7	ν_5	18.01112 ± 0.00049	0.228 ± 0.010	0.4957 ± 0.0073	14					
	TIC 197757000					TIC 240962482					TIC 241013310			
ν_1	36.65383 ± 0.00021	0.859 ± 0.016	0.3463 ± 0.0030	35	ν_1	27.98413 ± 0.00035	1.147 ± 0.016	0.2308 ± 0.0022	23	ν_1	5.72370 ± 0.00025	0.615 ± 0.014	0.9089 ± 0.0035	13
ν_2	29.57429 ± 0.00029	0.606 ± 0.016	0.9506 ± 0.0023	23	ν_2	27.65528 ± 0.00064	0.633 ± 0.016	0.5763 ± 0.0040	12	ν_2	6.25826 ± 0.00041	0.370 ± 0.014	0.3633 ± 0.0058	8
ν_3	26.64726 ± 0.00033	0.541 ± 0.016	0.4796 ± 0.0048	19	ν_3	27.29194 ± 0.00071	0.567 ± 0.016	0.0469 ± 0.0045	10	ν_3	14.76784 ± 0.00042	0.361 ± 0.014	0.4021 ± 0.0060	17
ν_4	21.64643 ± 0.00038	0.466 ± 0.016	0.2506 ± 0.0056	18	ν_4	29.43289 ± 0.00082	0.490 ± 0.016	0.9475 ± 0.0052	11	ν_4	4.81999 ± 0.00057	0.264 ± 0.014	0.4349 ± 0.0082	5
ν_5	38.32894 ± 0.00043	0.411 ± 0.016	0.3283 ± 0.0063	17	ν_5	24.96472 ± 0.00078	0.517 ± 0.016	0.7146 ± 0.0049	17					
	TIC 256640561					TIC 272822330					TIC 289947843			
ν_1	10.11866 ± 0.00018	0.217 ± 0.004	0.8581 ± 0.0028	36	ν_1	16.55851 ± 0.00001	0.506 ± 0.013	0.7901 ± 0.0042	11	ν_1	14.42411 ± 0.00003	0.359 ± 0.003	0.1029 ± 0.0013	52
ν_2	16.27639 ± 0.00037	0.105 ± 0.004	0.2941 ± 0.0057	19	ν_2	17.89061 ± 0.00001	0.471 ± 0.013	0.7731 ± 0.0045	10	ν_2	11.61637 ± 0.00004	0.251 ± 0.003	0.7666 ± 0.0019	32
ν_3	15.11399 ± 0.00039	0.100 ± 0.004	0.6635 ± 0.0060	19	ν_3	15.37946 ± 0.00001	0.332 ± 0.013	0.9197 ± 0.0064	8	ν_3	11.62279 ± 0.00005	0.201 ± 0.003	0.9408 ± 0.0024	26
ν_4	17.43972 ± 0.00043	0.090 ± 0.004	0.0847 ± 0.0067	16	ν_4	20.33903 ± 0.00001	0.326 ± 0.013	0.7286 ± 0.0065	7	ν_4	14.42924 ± 0.00007	0.164 ± 0.003	0.3675 ± 0.0030	24
ν_5	11.00822 ± 0.00063	0.062 ± 0.004	0.8177 ± 0.0097	10	ν_5	17.61348 ± 0.00001	0.306 ± 0.013	0.7254 ± 0.0070	6	ν_5	6.47827 ± 0.00007	0.145 ± 0.003	0.3530 ± 0.0033	14
	TIC 301909087					TIC 305633328					TIC 322428763			
ν_1	13.31209 ± 0.00019	2.861 ± 0.023	0.1732 ± 0.0013	39	ν_1	10.17360 ± 0.00037	0.806 ± 0.026	0.2727 ± 0.0052	19	ν_1	12.44685 ± 0.00002	27.487 ± 0.024	0.2984 ± 0.0001	380
ν_2	11.41486 ± 0.00041	1.341 ± 0.023	0.0983 ± 0.0028	25	ν_2	14.84142 ± 0.00043	0.699 ± 0.026	0.2635 ± 0.0060	18	$2\nu_1$	24.89370 ± 0.00013	3.479 ± 0.024	0.0780 ± 0.0011	81
ν_3	10.42865 ± 0.00057	0.964 ± 0.023	0.9806 ± 0.0038	20	ν_3	15.31862 ± 0.00055	0.541 ± 0.026	0.1905 ± 0.0078	15	$3\nu_1$	37.34056 ± 0.00038	1.223 ± 0.024	0.4383 ± 0.0031	54
ν_4	13.09508 ± 0.00061	0.896 ± 0.023	0.5211 ± 0.0041	13	ν_4	15.36912 ± 0.00094	0.320 ± 0.026	0.2315 ± 0.0132	9	ν_4	12.14721 ± 0.00062	0.749 ± 0.024	0.9277 ± 0.0050	11
ν_5	11.63832 ± 0.00068	0.803 ± 0.023	0.9980 ± 0.0046	14	ν_5	11.05172 ± 0.00119	0.253 ± 0.026	0.1454 ± 0.0166	5	$2\nu_1$–ν_4	12.74650 ± 0.00061	0.743 ± 0.024	0.7854 ± 0.0050	10
ν_1	23.65750 ± 0.00008	1.016 ± 0.030	0.3121 ± 0.0048	18	ν_1	8.26695 ± 0.00044	1.065 ± 0.023	0.2006 ± 0.0034	13	ν_1	27.06439 ± 0.00006	1.347 ± 0.024	0.0505 ± 0.0029	54
ν_2	24.50198 ± 0.00009	0.872 ± 0.030	0.7576 ± 0.0056	17	ν_2	18.46141 ± 0.00051	0.926 ± 0.023	0.3740 ± 0.0039	9	ν_2	23.55252 ± 0.00004	0.642 ± 0.015	0.5789 ± 0.0038	23
ν_3	22.90103 ± 0.00011	0.690 ± 0.030	0.4459 ± 0.0070	13	ν_3	10.20012 ± 0.00059	0.797 ± 0.023	0.5641 ± 0.0045	9	ν_3	24.96688 ± 0.00004	0.461 ± 0.014	0.8664 ± 0.0049	18
ν_4	23.56995 ± 0.00013	0.573 ± 0.030	0.6620 ± 0.0085	10	ν_4	18.83709 ± 0.00069	0.682 ± 0.023	0.8304 ± 0.0053	7	ν_4	28.51068 ± 0.00005	0.390 ± 0.014	0.3448 ± 0.0058	15
ν_5	30.96969 ± 0.00016	0.482 ± 0.030	0.2912 ± 0.0101	10	ν_5	14.87258 ± 0.00071	0.669 ± 0.023	0.2921 ± 0.0054	9	ν_5	27.09633 ± 0.00009	0.345 ± 0.018	0.6183 ± 0.0080	14

Table 4
(Continued)

	Frequency (day^{-1})	Amplitude (mmag)	Phase (rad)	S/N		Frequency (day^{-1})	Amplitude (mmag)	Phase (rad)	S/N		Frequency (day^{-1})	Amplitude (mmag)	Phase (rad)	S/N
	TIC 354926863					TIC 358613523					TIC 393894013			
ν_1	21.66089 ± 0.00002	1.813 ± 0.013	0.3126 ± 0.0011	89	ν_1	41.55243 ± 0.00024	0.465 ± 0.011	0.0551 ± 0.0039	24	ν_1	42.07023 ± 0.00056	0.468 ± 0.013	0.6493 ± 0.0043	14
ν_2	23.97610 ± 0.00010	0.311 ± 0.013	0.8778 ± 0.0064	15	ν_2	32.82261 ± 0.00036	0.309 ± 0.011	0.7414 ± 0.0058	17	ν_2	50.86278 ± 0.00060	0.444 ± 0.013	0.3516 ± 0.0045	15
ν_3	29.74307 ± 0.00011	0.291 ± 0.013	0.2144 ± 0.0068	20	ν_3	30.25640 ± 0.00038	0.298 ± 0.011	0.6099 ± 0.0060	16	ν_3	52.98499 ± 0.00074	0.359 ± 0.013	0.3011 ± 0.0056	13
ν_4	7.55377 ± 0.00011	0.278 ± 0.013	0.2867 ± 0.0071	15	ν_4	36.31599 ± 0.00047	0.240 ± 0.011	0.3481 ± 0.0075	13	ν_4	45.70912 ± 0.00077	0.345 ± 0.013	0.3654 ± 0.0058	12
ν_5	17.71561 ± 0.00013	0.238 ± 0.013	0.5979 ± 0.0084	14	ν_5	45.76655 ± 0.00050	0.224 ± 0.011	0.7536 ± 0.0080	14	ν_5	40.74380 ± 0.00087	0.305 ± 0.013	0.7169 ± 0.0066	10
	TIC 396134795					TIC 396201681					TIC 420114772			
ν_1	14.19761 ± 0.00025	2.507 ± 0.026	0.6492 ± 0.0016	31	ν_1	2.09187 ± 0.00003	3.890 ± 0.011	0.7970 ± 0.0004	90	ν_1	26.07772 ± 0.00012	0.402 ± 0.009	0.9829 ± 0.0035	35
ν_2	23.06211 ± 0.00052	1.190 ± 0.026	0.1993 ± 0.0035	20	ν_2	1.96327 ± 0.00004	3.284 ± 0.011	0.4973 ± 0.0005	72	ν_2	19.65159 ± 0.00012	0.400 ± 0.009	0.4690 ± 0.0035	34
ν_3	27.50727 ± 0.00087	0.711 ± 0.026	0.3443 ± 0.0058	9	ν_3	20.53793 ± 0.00006	1.973 ± 0.011	0.3971 ± 0.0009	93	ν_3	21.29354 ± 0.00012	0.390 ± 0.009	0.8579 ± 0.0036	36
ν_4	28.46996 ± 0.00097	0.637 ± 0.026	0.1605 ± 0.0065	8	ν_4	25.52245 ± 0.00008	1.433 ± 0.011	0.0180 ± 0.0012	68	ν_4	22.36688 ± 0.00014	0.338 ± 0.009	0.0937 ± 0.0041	32
ν_5	25.46129 ± 0.00162	0.380 ± 0.026	0.8832 ± 0.0109	8	ν_5	20.07776 ± 0.00014	0.873 ± 0.011	0.8036 ± 0.0020	48	ν_5	22.30157 ± 0.00015	0.300 ± 0.009	0.8503 ± 0.0047	28
	TIC 421714420					TIC 428003183					TIC 430808126			
ν_1	33.00852 ± 0.00001	0.566 ± 0.005	0.8806 ± 0.0013	94	ν_1	24.04691 ± 0.00025	0.921 ± 0.021	0.4706 ± 0.0037	21	ν_1	15.09493 ± 0.00029	0.808 ± 0.022	0.1633 ± 0.0043	22
ν_2	16.63040 ± 0.00001	0.223 ± 0.005	0.2679 ± 0.0033	38	ν_2	22.69924 ± 0.00051	0.592 ± 0.021	0.2310 ± 0.0074	15	ν_2	17.01396 ± 0.00030	0.780 ± 0.022	0.9924 ± 0.0045	21
ν_3	53.15438 ± 0.00001	0.172 ± 0.005	0.0092 ± 0.0043	33	ν_3	14.00456 ± 0.00040	0.590 ± 0.021	0.4984 ± 0.0058	14	ν_3	21.80517 ± 0.00044	0.540 ± 0.022	0.1305 ± 0.0064	12
ν_4	4.00603 ± 0.00001	0.114 ± 0.005	0.6070 ± 0.0066	17	ν_4	30.70567 ± 0.00044	0.532 ± 0.021	0.7363 ± 0.0064	11	ν_4	17.04825 ± 0.00047	0.501 ± 0.022	0.8969 ± 0.0069	11
ν_5	24.82455 ± 0.00001	0.101 ± 0.005	0.5483 ± 0.0073	14	ν_5	14.04931 ± 0.00066	0.458 ± 0.021	0.5547 ± 0.0096	11	ν_5	17.84270 ± 0.00057	0.416 ± 0.022	0.9987 ± 0.0084	10
ν_1	18.71653 ± 0.00031	1.204 ± 0.016	0.1117 ± 0.0021	36	ν_1	15.16456 ± 0.00003	2.646 ± 0.007	0.7014 ± 0.0004	167	ν_1	14.90235 ± 0.00001	3.905 ± 0.008	0.5206 ± 0.0004	166
ν_2	15.61934 ± 0.00032	1.192 ± 0.016	0.8186 ± 0.0021	36	ν_2	13.74681 ± 0.00005	1.468 ± 0.007	0.1107 ± 0.0008	82	ν_2	13.61211 ± 0.00001	3.039 ± 0.007	0.9023 ± 0.0005	152
ν_3	14.94367 ± 0.00040	0.940 ± 0.016	0.4500 ± 0.0027	29	ν_3	21.13332 ± 0.00006	1.226 ± 0.007	0.7881 ± 0.0009	58	ν_3	14.13054 ± 0.00001	2.320 ± 0.009	0.5640 ± 0.0005	97
ν_4	16.02039 ± 0.00054	0.697 ± 0.016	0.9872 ± 0.0036	21	ν_4	19.93937 ± 0.00009	0.852 ± 0.007	0.5775 ± 0.0013	46	ν_4	14.09850 ± 0.00001	1.035 ± 0.007	0.4843 ± 0.0011	43
ν_5	20.54519 ± 0.00058	0.657 ± 0.016	0.0864 ± 0.0038	20	ν_5	28.24970 ± 0.00009	0.809 ± 0.007	0.4093 ± 0.0014	46	ν_5	12.21896 ± 0.00001	0.702 ± 0.011	0.5071 ± 0.0019	51

Note. The full list of the frequencies is provided in electronic form.

(This table is available in its entirety in machine-readable form.)

ORCID iDs

F. Kahraman Aliçavuş https://orcid.org/0000-0002-9036-7476

References

Aerts, C., Christensen-Dalsgaard, J., & Kurtz, D. W. 2010, Asteroseismology, Astronomy and Astrophysics Library (Berlin: Springer)
Aerts, C., & Kolenberg, K. 2005, A&A, 431, 615
Amôres, E. B., & Lépine, J. R. D. 2005, AJ, 130, 659
Avvakumova, E. A., Malkov, O. Y., & Kniazev, A. Y. 2013, AN, 334, 860
Balona, L. A., Engelbrecht, C. A., Joshi, Y. C., et al. 2016, MNRAS, 460, 1318
Balona, L. A., & Ozuyar, D. 2020, MNRAS, 493, 5871
Baran, A. S., & Koen, C. 2021, AcA, 71, 113
Binnendijk, L. 1960, Properties of Double Stars: A Survey of Parallaxes and Orbits (Philadelphia, PA: Univ. Pennsylvania Press)
Borucki, W. J., Koch, D., Basri, G., et al. 2010, Sci, 327, 977
Breger, M., Stich, J., Garrido, R., et al. 1993, A&A, 271, 482
Budding, E., Erdem, A., Çiçek, C., et al. 2004, A&A, 417, 263
Choi, J., Dotter, A., Conroy, C., et al. 2016, ApJ, 823, 102
Dotter, A. 2016, ApJS, 222, 8
Dupret, M.-A., Grigahcène, A., Garrido, R., et al. 2005, A&A, 435, 927
Eker, Z., Soydugan, F., Bilir, S., et al. 2020, MNRAS, 496, 3887
Fuller, J., Kurtz, D. W., Handler, G., et al. 2020, MNRAS, 498, 5730
Gaia Collaboration, Brown, A. G. A., Vallenari, A., et al. 2021, A&A, 649, A1
Gray, D. F. 1992, Camb. Astrophys. Ser., Vol. 20
Handler, G., Kurtz, D. W., Rappaport, S. A., et al. 2020, NatAs, 4, 684
Kahraman Aliçavuş, F., Handler, G., Aliçavuş, F., et al. 2022, MNRAS, 510, 1413
Kahraman Aliçavuş, F., Soydugan, E., Smalley, B., et al. 2017, MNRAS, 470, 915
Kurtz, D. W., Handler, G., Rappaport, S. A., et al. 2020, MNRAS, 494, 5118
Lacy, M., Ridgway, S. E., Sajina, A., et al. 2015, ApJ, 802, 102
Lampens, P. 2021, Galax, 9, 28
Lenz, P., & Breger, M. 2005, CoAst, 146, 53
Liakos, A., & Niarchos, P. 2017, MNRAS, 465, 1181
Lovekin, C. C., & Guzik, J. A. 2017, ApJ, 849, 38
Mkrtichian, D. E., Kusakin, A. V., Rodriguez, E., et al. 2004, A&A, 419, 1015
Paxton, B., Bildsten, L., Dotter, A., et al. 2011, ApJS, 192, 3
Ricker, G. R., Winn, J. N., Vanderspek, R., et al. 2014, Proc. SPIE, 9143, 914320
Rodríguez, E., & Breger, M. 2001, A&A, 366, 178
Saio, H., Kurtz, D. W., Takata, M., et al. 2015, MNRAS, 447, 3264
Southworth, J. 2013, A&A, 557, A119
Southworth, J. 2021, Obs, 141, 282
Soydugan, E., İbanoğlu, C., Soydugan, F., et al. 2006, MNRAS, 366, 1289
Stassun, K. G., Oelkers, R. J., Paegert, M., et al. 2019, AJ, 158, 138
Svechnikov, M. A., & Kuznetsova, E. F. 2004, yCat, V/124
Tempesti, P. 1971, IBVS, 596, 1
Tody, D. 1986, Proc. SPIE, 627, 733
Uytterhoeven, K., Moya, A., Grigahcène, A., et al. 2011, A&A, 534, A125